Inorganic Chemistry

ARTICLE

pubs.acs.org/IC

Scaffolding, Ladders, Chains, and Rare Ferrimagnetism in Intermetallic Borides: Synthesis, Crystal Chemistry and Magnetism

Christian Goerens,[†] Jakoah Brgoch,[‡] Gordon J. Miller,[‡] and Boniface P. T. Fokwa*[,†]

[†]Institute of Inorganic Chemistry, RWTH Aachen University, Landoltweg 1, D-52064 Aachen, Germany, and

[‡]Department of Chemistry, Iowa State University, and Ames Laboratory, U.S. Department of Energy, Ames, Iowa 50011, United States

Supporting Information

ABSTRACT:

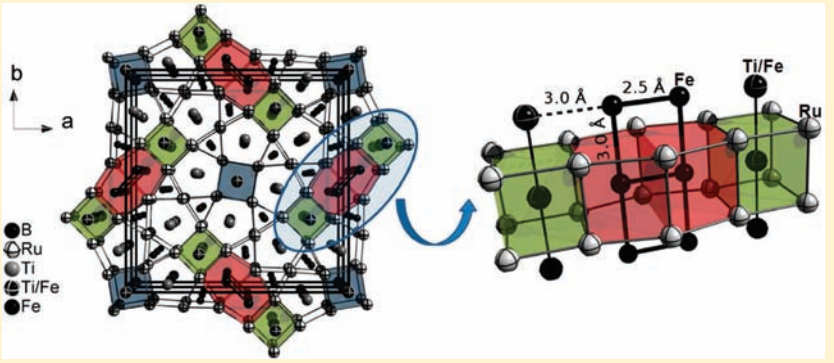

Single-phase polycrystalline samples and single crystals of the complex boride phases $Ti_8Fe_3Ru_{18}B_8$ and $Ti_7Fe_4Ru_{18}B_8$ have been synthesized by arc melting the elements. The phases were characterized by powder and single-crystal X-ray diffraction as well as energy-dispersive X-ray analysis. They are new substitutional variants of the $Zn_{11}Rh_{18}B_8$ structure type, space group *P*4/*mbm* (no. 127). The particularity of their crystal structure lies in the simultaneous presence of dumbbells which form ladders of magnetically active iron atoms along the [001] direction and two additional mixed iron/titanium chains occupying Wyckoff sites 4*h* and 2*b*. The ladder substructure is ca. 3.0 Å from the two chains at the 4*h*, which creates the sequence chain−ladder−chain, establishing a new structural and magnetic motif, the scaffold. The other chain (at 2*b*) is separated by at least 6.5 Å from this scaffold. According to magnetization measurements, $Ti_8Fe_3Ru_{18}B_8$ and $Ti_7Fe_4Ru_{18}B_8$ order ferrimagnetically below 210 and 220 K, respectively, with the latter having much higher magnetic moments than the former. However, the magnetic moment observed for $Ti_8Fe_3Ru_{18}B_8$ is unexpectedly smaller than the recently reported $Ti_9Fe_2Ru_{18}B_8$ ferromagnet. The variation of the magnetic moments observed in these new phases can be adequately understood by assuming a ferrimagnetic ordering involving the three different iron sites. Furthermore, the recorded hysteresis loops indicate a semihard magnetic behavior for the two phases. The highest H_c value (28.6 kA/m), measured for $Ti_7Fe_4Ru_{18}B_8$, lies just at the border of those of hard magnetic materials.

1. INTRODUCTION

Cooperative magnetic phenomena, such as ferromagnetism, ferrimagnetism, and antiferromagnetism, remain in the focus of condensed matter scientists for both experimentalists and theorists.[1−3] The ability to understand and predict the aforementioned magnetic properties is the goal of our research efforts. Intermetallic compounds and especially intermetallic borides are an ideal playground to reach this goal because the stoichiometry is so flexible that, for example, the valence electron count can be tuned by elemental substitution in a given structure type. We have performed several investigations on intermetallic magnets, where the relationship between electronic and structural factors was studied systematically. For instance, the itinerant magnets of the $Ti_3Co_5B_2$ structure type,[4] containing magnetically active elements in well-separated chains, turned out to be an excellent playground to tune the magnetic properties by adjusting the valence electron count (VEC). These new compounds exhibited a wide range of magnetic behavior ranging from Pauli-paramagnetism and antiferromagnetism to metamagnetism and ferromagnetism.[5−8] Other transition-metal borides, adopting the $Zn_{11}Rh_{18}B_8$ structure type which is related to the $Ti_3Co_5B_2$ structure type, also contain similar chains composed of a magnetically active element. One example is the compound series $Zn_{10}MRh_{18}B_8$ (M = Mn, Fe, Co, Ni),[9] although the magnetic properties of these compounds have not been published. Recently we reported on a new ferromagnet adopting the $Zn_{11}Rh_{18}B_8$ structure type, namely $Ti_9Fe_2Ru_{18}B_8$, which contains a remarkable substructure regarding the iron atoms,[1] i.e., well-separated chains of iron dumbbells. Such a ladder substructure has not been previously

Received: March 31, 2011
Published: June 02, 2011

Table 1. Rietveld Refinement Results for the Quaternary Borides $Ti_9Fe_2Ru_{18}B_8$, $Ti_8Fe_3Ru_{18}B_8$, and $Ti_7Fe_4Ru_{18}B_8$

	$Ti_9Fe_2Ru_{18}B_8$	$Ti_8Fe_3Ru_{18}B_8$	$Ti_7Fe_4Ru_{18}B_8$
space group; Z		*P4/mbm* (no. 127); 2	
lattice parameters (Å)	a = 17.525(3); c = 2.9678(5)	a = 17.519(2); c = 2.9670(4)	a = 17.487(2); c = 2.9621(3)
unit-cell volume(Å^3)	911.4(3)	910.6(2)	905.9(2)
θ range (°)		10.00° < θ < 90.00°	
refinement method		RIETVELD, least-squares method	
profile function		pseudo-Voigt	
structural model	$Ti_9Fe_2Ru_{18}B_8$ single-crystal data[1]	$Ti_8Fe_3Ru_{18}B_8$ single-crystal data with Ti/Fe: 2/1 at 4*h* and 2*b*	$Ti_8Fe_3Ru_{18}B_8$ single-crystal data with Ti/Fe: 1/2 at 4*h* and 2*b*
no. of refined parameters	52	52	52
R_{Bragg}	6.52	5.48	4.43
R_F	4.34	3.62	3.27

reported for a magnetically active 3d metal (Cr, Mn, Fe, Co, Ni) in intermetallic phases but does occur in AFe_2S_3 (A = K, Rb, Cs) compounds.[10] This ladder was found to be responsible for the ferromagnetic ordering of the $Ti_9Fe_2Ru_{18}B_8$ phase below ca. 200 K.

The desire to establish two different low-dimensional subunits in the same structure built up by a magnetically active element is the main idea behind this work: One-dimensional chains (as in the $Ti_3Co_5B_2$ structure type) and ladders (as in $Ti_9Fe_2Ru_{18}B_8$), interacting magnetically with each other.

The $Ti_9Fe_2Ru_{18}B_8$ structure also has a set of four different chains of titanium atoms, from which two (at Wyckoff sites 2*b* and 4*h*) are potential candidates for being substituted (partially or totally) by chains of magnetically active elements. These titanium atoms are found in a tetragonal prismatic environment of a 4d transition metal (ruthenium in this case), a coordination environment which was also found to accommodate iron in many phases of the $Ti_3Co_5B_2$ structure type, for example, in the $Sc_2FeRu_{5-n}Rh_nB_2$ series.[8a] Substitution at these sites will result in new substructures (chains) which may then give rise to several possibilities for the magnetic ordering, depending on their interaction with the iron ladder. The distances separating the ladders and the chains are such that magnetic interactions between these substructures are expected, with a strong potential to enhance the ferromagnetic ordering observed in $Ti_9Fe_2Ru_{18}B_8$ and to even achieve the rare ferrimagnetic ordering. In fact, two chains (at 4*h*) build together with the ladder substructure, the sequence chain-ladder-chain, thus enabling a new structural motif ("scaffold") for a magnetic element.

Here we report on the designed synthesis, the structural characterization, and the magnetic properties of the new complex intermetallic borides $Ti_8Fe_3Ru_{18}B_8$ and $Ti_7Fe_4Ru_{18}B_8$. A companion publication[11] focuses on the results of electronic structure calculations and magnetic ordering in these phases.

2. EXPERIMENTAL SECTION

2.1. Synthesis. Single-phase polycrystalline samples of $Ti_8Fe_3Ru_{18}B_8$ and $Ti_7Fe_4Ru_{18}B_8$ as well as single crystals of $Ti_8Fe_3Ru_{18}B_8$ were successfully synthesized by arc melting the elements in a water-cooled copper crucible under an argon atmosphere using a tungsten tip as a second electrode. The synthesis of "$Ti_6Fe_5Ru_{18}B_8$" was also attempted but the desired phase was not achieved. The starting materials, titanium (chunks, 99.9%, Degussa), iron (powder, 99.9%, ABCR), ruthenium (powder, 99.9%), and boron (crystalline pieces, 99.999%, Alfa Aesar) were weighed in the corresponding stoichiometric ratio (total mass 0.3 g), pressed into pellets, and arc melted under argon until homogeneous melting occurred. The argon was purified over silica gel, molecular sieves, and a titanium sponge (950 K). The products were turned and melted several times to ensure good homogeneity of the samples. Weight losses during the melting process were less than 1%. A product with metallic luster containing several needle-shaped crystals suitable for X-ray structure analysis was obtained. The product was stable in air both as a compact bulk and as a finely ground powder. The purity of each sample was checked by X-ray powder diffraction with the Guinier technique using Cu Kα_1 radiation (λ = 1.54059 Å). The presence of the metals and their ratios were characterized by energy-dispersive X-ray analysis (EDX) on a high-resolution, low-energy LEO 1530 SEM (Zeiss, Oberkochen, Germany) equipped with an INCA EDX system (Oxford Instruments). Averages of EDX measurements on several selected crystals agreed well with the ratios calculated from the metallic elements in the phases, although a small but noticeable deviation of the Ti:Fe ratio was observed: The obtained average Ti:Fe:Ru metal ratios were 1:0.36(3):2.23(1) and 1:0.53(3):2.55(1) for $Ti_8Fe_3Ru_{18}B_8$ and $Ti_7Fe_4Ru_{18}B_8$, respectively.

2.2. Structure Determination. Rietveld refinements were carried out not only for the two new phases but also for the already reported $Ti_9Fe_2Ru_{18}B_8$, using the FULLPROF[12]software. The results are reported in Table 1. The model used for the refinement of $Ti_7Fe_4Ru_{18}B_8$ was based on the single-crystal data of the $Ti_8Fe_3Ru_{18}B_8$ phase but modifying the composition accordingly. An example of the Rietveld plot for the $Ti_7Fe_4Ru_{18}B_8$ sample is shown in Figure 1.

The suitable single crystals found for the $Ti_8Fe_3Ru_{18}B_8$ composition were fixed on glass capillaries, and the data were collected using a CCD single-crystal diffractometer (Bruker Smart APEX) with graphite monochromatized Mo Kα radiation (λ = 0.71073 Å). Absorption correction was done using a semi-empirical procedure.[13] The crystal structure was solved by direct methods and refined by full-matrix least-squares refinement[14] based on F^2, using anisotropic displacement parameters for all of the metals (Ti, Fe, Ru) and isotropic parameters for boron. All relevant crystallographic data and experimental details concerning the data collection are listed in Table 2. Table 3 contains the atomic coordinates and displacement parameters, while Table 4 summarizes selected interatomic distances.

2.3. Magnetization Measurements. Magnetization measurements were performed on polycrystalline samples using a SQUID magnetometer (MPMS-5S, Quantum Design, San Diego, CA) in the temperature range of 4−300 K with applied fields up to 5 T. The data were corrected for the sample holder (Teflon tubes). Corrections for diamagnetic and conduction electron contributions were not applied.

3. RESULTS AND DISCUSSION

3.1. Phase Analysis and Structure Refinement. As in the synthesis of $Ti_9Fe_2Ru_{18}B_8$,[1] the two new $Ti_8Fe_3Ru_{18}B_8$ and

dx.doi.org/10.1021/ic200668j |*Inorg. Chem.* 2011, 50, 6289–6296

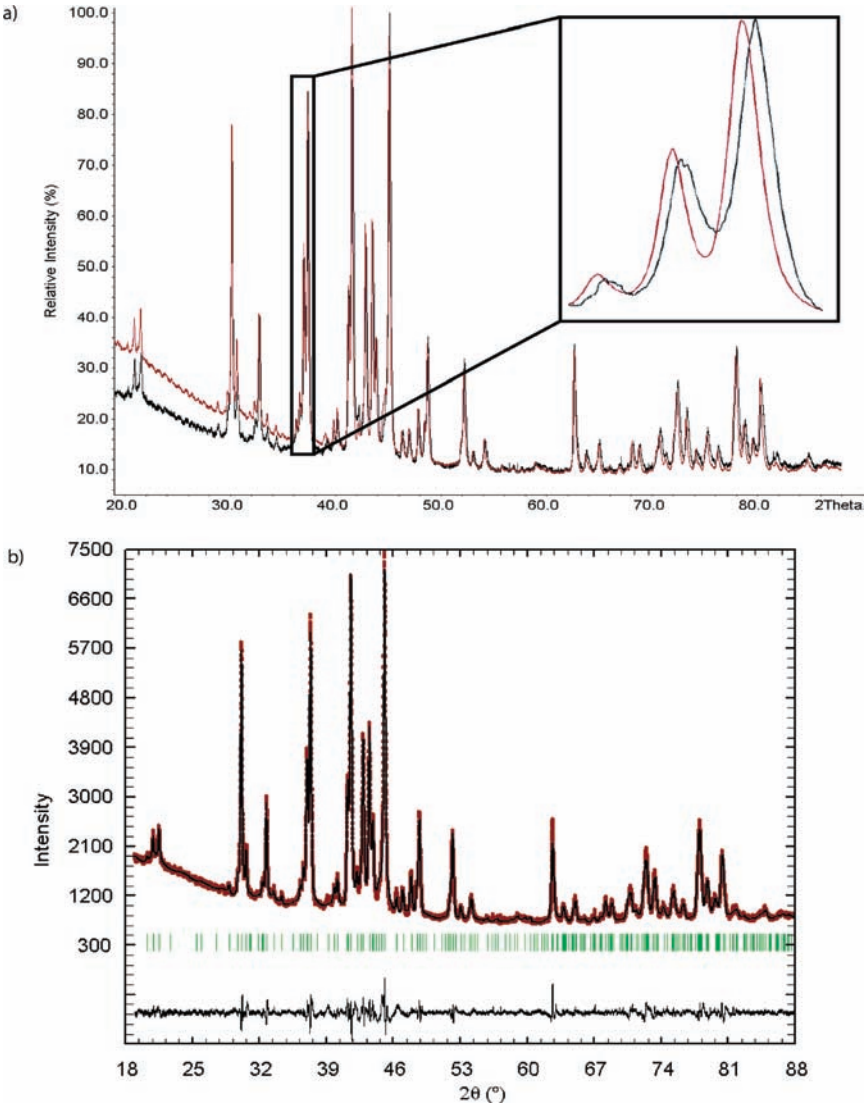

Figure 1. (a) Powder patterns of $Ti_8Fe_3Ru_{18}B_8$ (red curve) and $Ti_7Fe_4Ru_{18}B_8$ (black curve). The highlighted area is magnified in the upper right corner. (b) Rietveld refinement of the X-ray powder pattern of $Ti_7Fe_4Ru_{18}B_8$ showing measured and fitted intensities (top), the position of the Bragg peaks (middle), and the difference intensity curve (bottom).

$Ti_7Fe_4Ru_{18}B_8$ phases could be obtained as single phase. The structural model of the phase $Ti_9Fe_2Ru_{18}B_8$ was first used for the Rietveld refinements of the iron-rich phases; however, the intensities were not correctly matched. Also, the resulting lattice parameters were not only significantly smaller than those of the parent phase, but they also decrease with increasing iron amount (see Table 1), as expected when the larger titanium is substituted by the smaller iron [r_a(Ti) = 1.38 Å, half the bonding distance in the titanium metal, and r_a(Fe) = 1.25 Å].[15] There are four titanium sites in the $Ti_9Fe_2Ru_{18}B_8$ structure, which can be occupied by Fe. Of these four sites, two sit in pentagonal prisms and the other two in tetragonal prisms. Therefore, the probability of a size-dependent substitution is very high. Two models were developed to match the total amount of iron in the two phases: A statistical model, where all titanium sites were filled with both titanium and iron, and a size-dependent model, where only the tetragonal prisms were filled with both elements. Although the occupancies of the two elements could not be unequivocally refined from these powder data, the results for both compounds clearly favor the size-dependent model. Single-crystal refinement was then necessary for the validation of this model and for the determination of the titanium and iron occupancies on the mixed sites.

Fortunately, some single crystals were obtained from both samples, but only one originating from the iron-poor composition was good enough for single-crystal refinements. The standardized $Ti_9Fe_2Ru_{18}B_8$ structure[1a] was used as a starting model for the single-crystal structure refinements. After a few refinement cycles, the structure type was confirmed. However, a careful inspection of the displacement parameters of all atoms revealed that those of two of the four available titanium positions were unusually small suggesting more electron density on these two sites. Because EDX analysis and powder X-ray diffraction (single-phase products and smaller lattice parameters) suggested that the amount of iron should be higher than in $Ti_9Fe_2Ru_{18}B_8$, a titanium/iron mix-occupancy refinement was applied on all titanium sites. However, iron could be found together with titanium only on the above-mentioned two (2*b* and 4*h*) Wyckoff

dx.doi.org/10.1021/ic200668j |*Inorg. Chem.* 2011, 50, 6289–6296

Table 2. Crystallographic and Structure Refinement Data for $Ti_{8.1(1)}Fe_{2.9}Ru_{18}B_8$

formula	$Ti_{8.1(1)}Fe_{2.9}Ru_{18}B_8$
formula weight (g/mol); F(000)	2455.58; 2171
space group; Z	*P4/mbm* (N°. 127); 2
lattice parameters (Å)	a = 17.519(2); c = 2.9670(4)
unit-cell volume (Å^3)	910.6(2)
calculated density (g/cm^3)	8.97
absorption correction	semi-empirical
absorption coefficient (mm^{-1})	19.98
diffractometer	Bruker APEX CCD, Mo Kα, graphite monochromator
Θ range (°)	4.80° < θ < 35.83°
hkl ranges	$-28 \le h \le 26$ $-28 \le k \le 26$ $-4 \le l \le 4$
no. of reflections; R_{int}	9564; 0.051
no. of independent reflections	1241
no. of parameters	57
refinement method	SHELXL-97, full matrix against F^2
R_1; wR_2 (all I)	0.0396; 0.0556
goodness of fit	1.074
diffraction peak and hole (e/Å^3)	1.988/−2.017

Table 3. Atomic Coordinates and Displacement Parameters (Å^2) for $Ti_{8.1(1)}Fe_{2.9}Ru_{18}B_8$

atom	Wyckoff site	x	y	z	occupancy	U_{eq}[a]
Ru1	8*i*	0.91920(2)	0.25288(2)	1/2	1	0.0042(1)
Ru2	4*g*	0.91545(2)	0.41545(2)	1/2	1	0.0042(1)
Ru3	8*i*	0.93039(2)	0.09699(2)	1/2	1	0.0044(1)
Ru4	8*i*	0.05297(2)	0.32561(2)	1/2	1	0.0052(1)
Ru5	8*i*	0.78786(2)	0.16823(2)	1/2	1	0.0050(1)
Ti1	4*h*	0.80345(6)	0.30345(6)	0	1	0.0065(2)
Ti2	8*j*	0.03505(6)	0.18682(6)	0	1	0.0062(2)
Ti3/Fe3	4*h*	0.17181(5)	0.32819(5)	0	0.74(3)/0.26	0.0062(3)
Ti4/Fe4	2*b*	0	0	0	0.63(4)/0.37	0.0048(4)
Fe1	4*h*	0.05079(5)	0.44921(5)	0	1	0.0062(2)
B1	8*j*	0.8778(3)	0.1691(3)	0	1	0.0058(10)
B2	8*j*	0.9625(3)	0.3342(3)	0	1	0.0052(10)

[a] U_{eq} is defined as one-third of the trace of the orthogonalized U_{ij} tensor. For boron, U_{eq} is the isotropic thermal parameter (U_{iso}).

sites after convergence of the refinement (see Table 3), thereby confirming the size-dependent model. The refined composition was richer in iron than in the $Ti_9Fe_2Ru_{18}B_8$ case and leads to the final composition $Ti_{8.1(1)}Fe_{2.9}Ru_{18}B_8$. A site preference between the Ti/Fe mixing also was investigated. Although 10(4) % more iron is located at 2*b* than at 4*h*, due to the large standard deviations, no significant site preference can be determined between the sites. However, as observed in $Ti_9Fe_2Ru_{18}B_8$ electronic reasons may be decisive. A similar result is also obtained from electronic structure calculations: Although the electron counts of the two sites are very similar, there is a slight

Table 4. Selected Interatomic Distances in $Ti_{8.1(1)}Fe_{2.9}Ru_{18}B_8$

		d_{min} (Å)	d_{max} (Å)
Ru	B	2.153(4)	2.213(4)
	Ti	2.662(1)	2.863(2)
	Ti/Fe	2.515(2)	2.562(1)
	Fe	2.623(1)	2.856(1)
	Ru	2.666(1)	2.965(1)
Fe	Fe	2.514(2)	2.965(1)
Ti/Fe	Ti/Fe	–	2.965(1)
	Fe	–	2.996(2)
	Ti	3.259(2)	3.443(2)

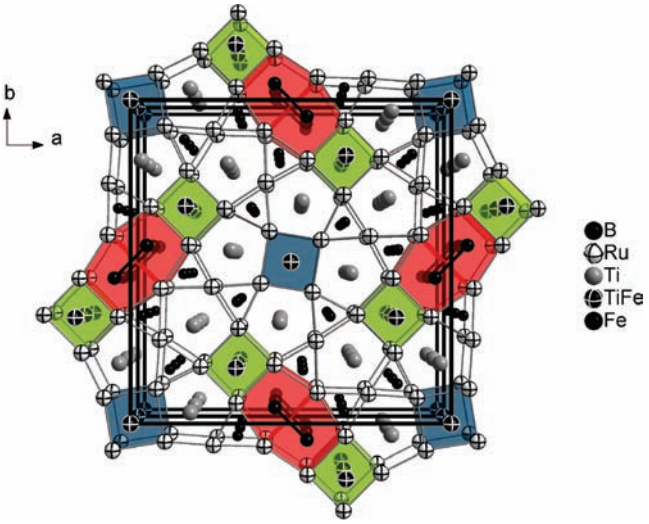

Figure 2. Projection of the crystal structure of $Ti_8Fe_3Ru_{18}B_8$ and $Ti_7Fe_4Ru_{18}B_8$ phases along the [001] direction. Polyhedra around the iron-containing sites are highlighted: Ti/Fe on 2*b* site (blue); Ti/Fe on 4*h* site (green); and Fe on another 4*h* site (red).

site preference for a more electron-rich atom to occupy the 2*b*-chain site (see the companion publication[11] for details).

A Rietveld refinement based on the single-crystal data of $Ti_{8.1(1)}Fe_{2.9}Ru_{18}B_8$ was applied for the $Ti_7Fe_4Ru_{18}B_8$ phase because no suitable single crystal could be obtained as mentioned above. Given the negligible site preference in the two mixed sites in $Ti_{8.1(1)}Fe_{2.9}Ru_{18}B_8$, a statistical Ti/Fe occupation of these sites (33/67% for each) was successfully used in this refinement (see Table 1 and Figure 1). In some areas peak profile fitting is insufficient in this complex powder pattern. In fact, the peaks are slightly broadened; this is probably due to a small phase width, which can be expected because of the competition in site occupations observed between the two Ti/Fe sites (described above). In this iron richest phase, iron is the main component in both mixed chains and, thus, affects the magnetic properties of $Ti_9Fe_2Ru_{18}B_8$ to a greater extent than in the previous case ($Ti_8Fe_3Ru_{18}B_8$), where titanium prevails in the mixed sites (see the Magnetism Section).

To conclude this section, the single-phase nature of the powder samples, the significantly smaller lattice parameters, the semiquantitative EDX analyses, and the single-crystal refinement results indeed confirm the successful synthesis of the two $Ti_8Fe_3Ru_{18}B_8$ and $Ti_7Fe_4Ru_{18}B_8$ phases. Because the two phases

dx.doi.org/10.1021/ic200668j |*Inorg. Chem.* 2011, 50, 6289–6296

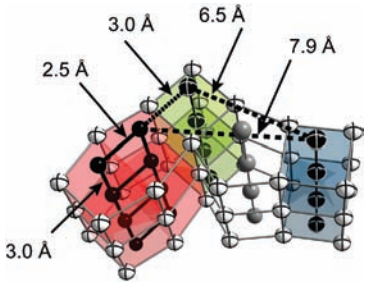

Figure 3. Iron ladder (in the red channel), Ti/Fe mixed chains (in the green and blue channels), and distances between the three iron-containing substructures in the $Ti_8Fe_3Ru_{18}B_8$ compound.

Table 5. Magnetic Quantities for $Ti_8Fe_3Ru_{18}B_8$ and $Ti_7Fe_4Ru_{18}B_8$

	$Ti_8Fe_3Ru_{18}B_8$	$Ti_7Fe_4Ru_{18}B_8$
T_C (K)	210	220
μ_a (μ_B), at 5 T and 5 K	0.868	1.814
H_C (kAm^{-1})	10.3	28.6
Curie–Weiss Range (K)	210–300	220–300
θ (K)	95	169
C ($m^3 \cdot K \cdot mol^{-1}$)	3.59×10^{-4}	3.35×10^{-4}

have the same structure model compared to $Ti_9Fe_2Ru_{18}B_8$ phase, they may be generalized by the formula $Ti_{9-n}Fe_{2+n}Ru_{18}B_8$ ($n = 1, 2$).

3.2. Crystal Chemistry. Figure 2 shows a perspective view of the crystal structure of $Ti_{9-n}Fe_{2+n}Ru_{18}B_8$ (n = 1, 2) phases, which belongs to the $Zn_{11}Rh_{18}B_8$-type, space group $P4/mbm$ (no. 127). This structure is built up by trigonal, tetragonal, pentagonal, and elongated hexagonal prisms of Ru atoms stacked on top of each other, thus building channels along the [001] direction. Here boron atoms center the trigonal prisms, the pentagonal prisms accommodate the titanium atoms, and the elongated hexagonal prisms contain the Fe_2 dumbbells which build a ladder substructure along the [001] direction. The centers of the tetragonal prisms at Wyckoff sites 2*b* and 4*h*, however, are filled by two different mixtures of titanium and iron atoms, resulting in two chains of Ti/Fe atoms along [001]. Compared with the structure of the isotypic $Ti_9Fe_2Ru_{18}B_8$, iron is found together with titanium at only two of the four titanium chains generating two Ti/Fe chains. The distances from the two mixed chains (at 2*b* and 4*h*) to the iron ladder are 7.9 and 3.0 Å, respectively. Therefore, based on these distances a direct magnetic interaction is only expected between the iron ladder and the mixed chain at the 4*h* sites. In fact, two mixed chains at 4*h* sandwich the iron ladder to build a "scaffold", which is a new structural unit for a magnetically active element (red and blue units of Figure 2). As a result, the magnetic properties found in $Ti_9Fe_2Ru_{18}B_8$ likely will be strongly perturbed, depending on the interactions of these mixed Ti/Fe chains with the iron ladder. However, the two Ti/Fe mixed chains (blue and green chains in Figures 2 and 3) are separated by 6.5 Å, and consequently no significant direct or through-space interactions are expected.

All of the bond distances in $Ti_8Fe_3Ru_{18}B_8$ are not only in the same range as those observed in the isotypic $Ti_9Fe_2Ru_{18}B_8$,[1] $Ti_{10}Ru_{19}B_8$,[16a] and $Ti_9M_2Ru_{18}B_8$ (M = Cr, Mn, Co–Zn) phases,[16b] but they are also comparable to those found in other borides containing at least three of the elements used: $Ti_{1.6}Os_{1.4}RuB_2$[17]

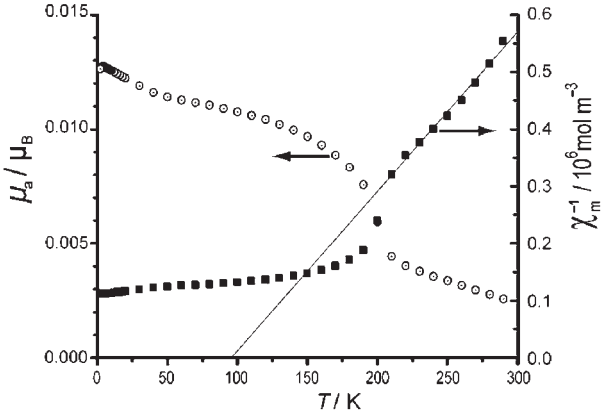

Figure 4. Atomic magnetic dipole moment (white circles) and reciprocal susceptibility (black squares) as functions of temperature at an applied field of 0.01 T for $Ti_8Fe_3Ru_{18}B_8$.

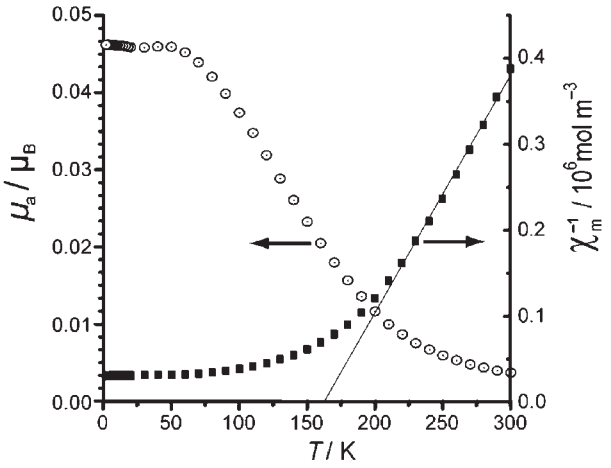

Figure 5. Atomic magnetic dipole moment (white circles) and reciprocal susceptibility (black squares) as functions of temperature at an applied field of 0.01 T for $Ti_7Fe_4Ru_{18}B_8$.

and $Fe_xRu_{7-x}B_3$ ($0 < x \leq 1.5$).[18] In the isotypic $Ti_9M_2Ru_{18}B_8$ (M = Cr–Zn) phases, the heteroatomic Ru–B and Ru–Ti interactions were found to be mainly responsible for their structural stability. In the new phases, these heteroatomic interactions are also the main structural stabilizing factors, as found by crystal orbital Hamilton population (COHP) bonding analysis of the hypothetical "$Ti_{8.5}Fe_{2.5}Ru_{18}B_8$" phase, which also belongs to the $Ti_{9-n}Fe_{2+n}Ru_{18}B_8$ series. A detailed chemical bonding analysis is given in a companion publication (theoretical section).[11] The bond distances in $Ti_7Fe_4Ru_{18}B_8$, obtained from the Rietveld analysis follows the trend imposed by the lattice parameters and are thus shorter than in the two iron poorer phases. Earlier investigations on the $Ti_9Fe_2Ru_{18}B_8$ compound made clear that, in terms of volume, one-half of the elongated hexagonal prism (i.e., the volume accommodating only one atom of the dumbbell) is smaller than a single pentagonal prism but larger than a tetragonal prism. The fact that the iron atoms occupy the hexagonal prism in the $Ti_9Fe_2Ru_{18}B_8$ compound cannot be explained by size factors, and electronic reasons are playing a key role. As for the new compounds discussed here, size factors seem to play an important role regarding the additional

dx.doi.org/10.1021/ic200668j |*Inorg. Chem.* 2011, 50, 6289–6296

iron atoms incorporated into the $Ti_9Fe_2Ru_{18}B_8$ structure. The additional iron atoms (mixed with titanium atoms on their sites) are found exclusively at the centers of the smaller tetragonal prisms of ruthenium atoms, while the larger pentagonal prisms are filled by the larger titanium atoms.

3.3. Magnetism. Magnetization measurements on the $Ti_9Fe_2Ru_{18}B_8$ compound revealed a ferromagnetic ordering between 10 and 200 K. The model for ferromagnetism in this ladder-based structure was identified to be a ferromagnetic coupling among neighboring spin−triplet Fe_2 dimers along the *c* axis. Table 5 summarizes the key magnetic quantities for the new $Ti_8Fe_3Ru_{18}B_8$ and $Ti_7Fe_4Ru_{18}B_8$ phases. Figures 4 and 5 show both the magnetic dipole moment vs temperature ($\mu_a - T$) and the reciprocal molar susceptibility vs temperature ($\chi_m^{-1} - T$) curves at 0.01 T for the $Ti_8Fe_3Ru_{18}B_8$ and $Ti_7Fe_4Ru_{18}B_8$ phases, respectively. The presentation of the magnetic data follows the recommendation of Hatscher et al. (SI units).[19]

The $\chi_m^{-1} - T$ curves for the $Ti_8Fe_3Ru_{18}B_8$ (Figure 4) and $Ti_7Fe_4Ru_{18}B_8$ (Figure 5) phases show Curie−Weiss behaviors for the temperature ranges 210−300 and 220−300 K, respectively. Weiss constants were found to be $\theta = +94$ and $+169$ K for both structures as well, indicating that ferromagnetic interactions dominate in the two phases. From the $\mu_a - T$ curves, magnetic ordering temperatures of 210 and 220 K are derived, which are only slightly larger than the 200 K found for the ferromagnetic $Ti_9Fe_2Ru_{18}B_8$ phase. The value of T_C was deduced from the intersection of a linear fit to the steepest part of the magnetization curve with the temperature axis at low applied fields ($\leq$0.1 T). The observed Curie temperatures and the positive Weiss constants clearly exclude antiferromagnetic or metamagnetic orderings for the two new phases. The magnetic ordering in these phases may, therefore, be either ferro- or ferrimagnetic, because in addition to the iron ladder (present in $Ti_9Fe_2Ru_{18}B_8$) two other sites containing iron (Ti/Fe sites) are found in the crystal structures of the iron-richer phases. In the case of ferromagnetic ordering the total magnetic moment must increase relative to $Ti_9Fe_2Ru_{18}B_8$, whereas a ferrimagnetic ordering may either increase or decrease the moment. Therefore, from these magnetic measurements, a ferrimagnetic ordering will only be safely proven if the total magnetic moment of the phase is lower than that of $Ti_9Fe_2Ru_{18}B_8$.

For $Ti_9Fe_2Ru_{18}B_8$, measurements of the atomic magnetic dipole moment (μ_a) vs applied field (at 5 K) showed that a small field (0.05 T) was needed to obtain a μ_a value of 0.300 μ_B. At a high field (5 T), saturation was still not achieved, and a μ_a value of 0.885 μ_B was measured. For $Ti_8Fe_3Ru_{18}B_8$ a $\mu_a = 0.868$ μ_B at 5 T and 5 K can be determined, which is 0.017 μ_B smaller than in $Ti_9Fe_2Ru_{18}B_8$. Upon further iron substitution, en route to $Ti_7Fe_4Ru_{18}B_8$, μ_a dramatically increases to 1.814 μ_B. Can we understand these two different behaviors?

As stated above, a decrease of the magnetic moment in $Ti_8Fe_3Ru_{18}B_8$ is well explained by assuming ferrimagnetic ordering between the three different iron containing sites, i.e., assuming that both ferromagnetic and antiferromagnetic interactions are present. One way to achieve ferrimagnetic ordering with a smaller total magnetic moment than that of $Ti_9Fe_2Ru_{18}B_8$ phase (Figure 6a) is to assume: (a) ferromagnetic interactions in the iron ladder, (b) ferromagnetic interactions in the mixed chain (at 4*h*) interacting antiferromagnetically with the iron ladder, and (c) antiferromagnetic interactions in the other mixed Ti/Fe chain (at 2*b*). This means that the total magnetic moment of the phase will come from the scaffold unit (chain−ladder−chain) because the

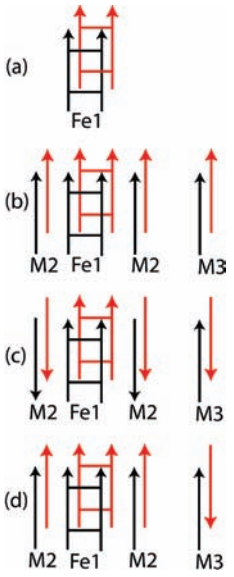

Figure 6. Some magnetically ordered models for $Ti_{9-n}Fe_{2+n}Ru_{18}B_8$ series: (a) The ferromagnetic model for $n = 0$; (b) the least probable ferromagnetic model for $n = 1, 2$; (c) the proposed ferrimagnetic model for $n = 1$; and (d) the proposed ferrimagnetic model for $n = 2$. The arrows indicate the orientations of the magnetic moments for the Fe1 (ladder), M2 (Ti3/Fe3, 4*h* chain), and M3 (Ti4/Fe4, 2*b* chain) sites. The two different colors signify two different unit cells along the [001] direction. The sizes of all arrows are arbitrary.

mixed chain at 2*b* is isolated and should produce a zero moment (antiferromagnetic interactions in the chain, see Figure 6c for a sketch of the proposed model). Furthermore, the fact that titanium prevails in the two Ti/Fe mixed chains in the $Ti_8Fe_3Ru_{18}B_8$ structure indicates that these sites will carry much smaller magnetic moments than the iron ladder, and thus the total magnetic moment of the phase will be closer to that of $Ti_9Fe_2Ru_{18}B_8$, as mentioned above. In fact, the ferrimagnetic ordering and the decrease of the magnetic moment in the phase are also supported by density functional theory (DFT) calculations on different magnetic models using the Simpsońs integration method (see DFT calculations published in ref 11).

In the $Ti_7Fe_4Ru_{18}B_8$ phase, the total magnetic moment is more than double the magnetic moment of $Ti_9Fe_2Ru_{18}B_8$. Again, either ferro- or ferrimagnetic ordering can be assumed. However, ferromagnetic ordering is unlikely in this phase, particularly because until now all ruthenium-rich phases containing "isolated" chains of iron atoms were found to be dominated by antiferromagnetic exchange interactions in the chains, for example, Fe−Fe antiferromagnetic interactions in the $Sc_2FeRu_{5-n}Rh_nB_2$ ($n = 0, 1, 2$) phases[1a] and in $Zr_2Fe_{5-\delta}(Ru_{1-x}Rh_x)_{5+\delta}B_2$ ($x = 0.2$ ca. $\delta = 0.1$).[20] Because iron is the main component in the mixed Ti/Fe chains of this phase, a similar behavior is expected for the "isolated" chain (2*b* site). Assuming an antiferromagnetic ordering of this isolated chain, an increase of the total magnetic moment can only be explained by a ferromagnetic interaction between the remaining two interacting units (the Ti/Fe chain at 4*h* and the Fe ladder, see Figure 6d for a sketch of the proposed model), thereby leading to a strong ferrimagnet. Also here the DFT calculations have predicted ferrimagnetic ordering to be more energetically favorable than the ferromagnetic case.[11] However the trend in total magnetic moment differs from the experimental findings, but this is likely due to changes which stem

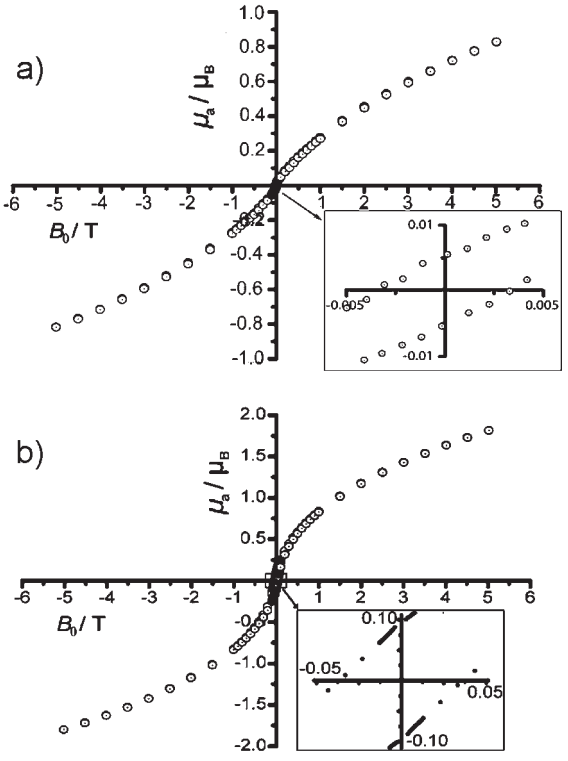

Figure 7. Hysteresis loops for: (a) $Ti_8Fe_3Ru_{18}B_8$ and (b) $Ti_7Fe_4Ru_{18}B_8$ at 10 K. Inset: Enlarged part of the hysteresis showing the coercive field and the remanence.

from differences in mixed Ti/Fe occupancies at the two Ti/Fe sites, as stated above. The effect of atomic mixing on long-range magnetic ordering is currently under investigation.

The low-temperature behavior of the phase $Ti_9Fe_2Ru_{18}B_8$ indicated a possible second magnetic ordering near 4 K due to the presence of a broad maximum in the $\mu_a - T$ curve. This broad maximum is also observed at nearly the same temperature in the $Ti_8Fe_3Ru_{18}B_8$ phase. In the iron-richest $Ti_7Fe_4Ru_{18}B_8$ phase, however, a broad maximum is also observed but at around 70 K, possibly also a second magnetic ordering. The present data do not allow a safe explanation of the low-temperature behavior. Therefore ferrimagnetic ordering exists in $Ti_8Fe_3Ru_{18}B_8$ phase over the temperature range of 10−210 K, and over the temperature range of 75−220 K in $Ti_7Fe_4Ru_{18}B_8$ phase. Mössbauer and neutron diffraction experiments (at temperatures below 75 K) are planned to investigate the low-temperature behavior in all three phases.

Special attention was finally devoted to the hysteresis measurements performed at 10 K and applied fields at $-5\ \mathrm{T} \le B_0 \le +5\ \mathrm{T}$. The measured hysteresis loops (μ_a vs B_0) for both phases do not saturate up to the highest measured field of 5 T (see Figure 7). From these hysteresis loops the coercivities, H_c, have been calculated in order to classify the magnetic hardness of these materials ($H_c < 1\ \mathrm{kAm^{-1}}$ stands for 'soft' and $H_c > 30\ \mathrm{kAm^{-1}}$ for 'hard').[2,3] The calculated coercivities of both phases lie between 1 and 30 $\mathrm{kAm^{-1}}$ (Table 5) and are therefore in the range of semihard magnetic materials, with the iron-richest phase being even closer to a hard ferrimagnet. It was recently found that the presence of titanium in a Ru-rich boride phase may be the driving force to a hysteresis enlargement in the family of transition-metal-rich borides.[21] This effect was observed when studying the magnetic properties of the $Ti_2FeRu_{5-n}Rh_nB_2$ ($n = 1 - 5$, VEC = 63−67) series[21] as a function of the valence electron count (VEC). In fact, an evolution from soft to semihard ferromagnetic materials was obtained when decreasing VEC from 67 to 63, that is, by increasing the ruthenium content. This behavior was not observed in the homologous $Sc_2FeRu_{5-n}Rh_nB_2$ ($n = 0 - 5$, VEC = 60−65),[8] where only soft magnetic materials were reported at the same VECs (63−65) as in the Ti-based series. Thus, both titanium and ruthenium are indeed playing a crucial role in this hysteresis enlargement process.

4. CONCLUSIONS

We have successfully synthesized the new phases $Ti_8Fe_3Ru_{18}B_8$ and $Ti_7Fe_4Ru_{18}B_8$, which are new substitutional variants of the $Zn_{11}Rh_{18}B_8$ structure type. They were characterized using powder and single-crystal X-ray analysis as well as EDX measurements. Both phases contain besides a ladder substructure built up by the magnetically active iron atoms, two additional one-dimensional chains composed of titanium and iron atoms, with only one of the chains directly interacting with the iron ladder thereby building a scaffold unit (chain−ladder−chain). Magnetization measurements suggest ferrimagnetic ordering for the two phases below 210 and 220 K, respectively. According to their coercive fields, the new phases show semihard magnetic behavior. Theoretical models based on the hypothetical "$Ti_6Fe_5Ru_{18}B_8$" with iron fully occupying the two one-dimensional chain sites in combination with a rigid-band approach correctly predict the preferred magnetic structure for all of the structures discussed here. In fact, at low-iron content, i.e., $Ti_9Fe_2Ru_{18}B_8$, ferromagnetic ordering is predicted, whereas ferrimagnetic ordering is predicted for the iron-richer substitution, i.e., $Ti_8Fe_3Ru_{18}B_8$ and $Ti_7Fe_4Ru_{18}B_8$. In all three cases the theoretical calculations help to confirm the results found experimentally.

■ ASSOCIATED CONTENT

Ⓢ Supporting Information. This material is available free of charge via the Internet at http://pubs.acs.org.

■ AUTHOR INFORMATION

Corresponding Author
*E-mail: boniface.fokwa@ac.rwth-aachen.de.

■ ACKNOWLEDGMENT

The authors wish to acknowledge the generous financial support through a joint grant provided by the Deutsche Forschungsgemeinschaft (Germany) and the National Science Foundation (USA; NSF DMR 05-02671 and 08-06507) through the Materials World Network program. We also thank Ms. Resi Zaunbrecher (IPC, RWTH-Aachen) for the EDX analyses, Mr. Klaus Kruse and Dr. Paul Müller for various X-ray data collections. C.G. thanks the National Research Fund, Luxembourg, for awarding him a Ph.D. fellowship.

■ REFERENCES

(1) (a) Fokwa, B. P. T.; Samolyuk, G. D.; Miller, G. J.; Dronskowski, R. *Inorg. Chem.* **2008**, *47* (6), 2113. (b) Fokwa, B. P. T. *Eur. J. Inorg. Chem.* **2010**, 3075.
(2) Lueken, H. *Magnetochemie*; Teubner: Stuttgart, Germany, 1999.
(3) Chikazumi, S. *Physics of Ferromagnetism*; Clarendon Press: Oxford, U.K., 1997.

(4) Kuz'ma, Y. B.; Yarmolyuk, Y. P. *Zh. Strukt. Khim.* **1971**, *12*, 458.
(5) Nagelschmitz, E. A.; Jung, W. *Chem. Mater.* **1998**, *10*, 3189.
(6) (a) Nagelschmitz, E. A.; Jung, W.; Feiten, R.; Müller, P.; Lueken, H. *Z. Anorg. Allg. Chem.* **2001**, *627*, 523.(b) Nagelschmitz, E. A. *Ph.D. Disseration*, University of Cologne: Cologne, Germany, 1995. (c) Feiten, R. *Ph.D. Dissertation*, RWTH Aachen University: Aachen, Germany, 1996.
(7) (a) Dronskowski, R.; Korczak, K.; Lueken, H.; Jung, W. *Angew. Chem.* **2002**, *114*, 2638. (b) Dronskowski, R.; Korczak, K.; Lueken, H.; Jung, W. *Angew. Chem., Int. Ed.* **2002**, *41*, 2528.
(8) (a) Fokwa, B. P. T.; Lueken, H.; Dronskowski, R. *Chem.—Eur. J.* **2007**, *13*, 6040. (b) Samolyuk, G. D.; Fokwa, B. P. T.; Dronskowski, R.; Miller, G. J. *Phys. Rev. B* **2007**, *76*, 094404.
(9) Eibenstein, U.; Jung, W. *Z. Anorg. Allg. Chem.* **1998**, *624*, 802.
(10) Mitchell, R. H.; Ross, K. C.; Potter, E. G. *J. Solid State Chem.* **2004**, *177*, 1867.
(11) Brgoch, J.; Goerens, C.; Fokwa, B. P. T.; Miller, G. J. *J. Am. Chem. Soc.* **2011**, *133*, 6832.
(12) Rodriguez-Caravajal J. *Fullprof*, version 3.2; Laboratoire Léon Brillouin: XXX1997.
(13) Sheldrick, G. M. SADABS; University of Göttingen: Göttingen, Germany, 2001.
(14) Sheldrick, G. M. *Acta Crystallogr.* **2008**, *A64*, 112.
(15) Pauling, L.; Kamb *B. Proc. Natl. Acad. Sci. U.S.A.* **1986**, *83*, 3569.
(16) (a) Fokwa, B. P. T. *Z. Anorg. Allg. Chem.* **2009**, *635*, 2258. (b) Fokwa, B. P. T.; Goerens, C.; Gillessen, M. *Z. Kristallogr.* **2010**, *225*, 180.
(17) Fokwa, B. P. T.; von Appen, J.; Dronskowski, R. *Chem. Commun.* **2006**, 4419.
(18) Fokwa, B. P. T.; Dronskowski, R. *J. Alloys Compd.* **2007**, *428*, 84.
(19) Hatscher, S. T.; Schilder, H.; Lueken, H.; Urland, W. *Pure Appl. Chem.* **2005**, *77*, 497.
(20) Brgoch, J.; Yeninas, S.; Prozorov, R.; Miller, G. J. *J. Solid State Chem.* **2010**, *183*, 2917–2924.
(21) Fokwa, B. P. T.; Lueken, H.; Dronskowski, R. *Eur. J. Inorg. Chem.* **2011**, DOI: 10.1002/ejic.201100315.